Inversion of *EM38* Electrical Conductivity Data

Ernesto Bonomi, Cristina Manzi and Enrico Pieroni
Center of Advanced Studies, Research and Development in Sardinia
Environmental and Imaging Sciences Group
C.P. 94, I-09010 Uta, Italy

Gian Piero Deidda
University of Cagliari, Department of Territorial Engineering
Piazza D'Armi 16, I-09123 Cagliari, Italy

July 5, 2001

Abstract

In geophysical prospecting and environmental monitoring, the frequency domain electromagnetic induction technique has been developed for measuring the apparent soil electrical conductivity. A linear model can be formulated to describe the response of the *EM38*, a ground conductivity meter. To image the subsurface conductivity profile from recorded data, the model has been inverted defining a Least Squares problem with Tikhonov regularization. The resulting linear systems are solved by a projected conjugate gradient algorithm. Numerical results have shown that, although Tikhonov approach improves the conditioning of the resulting linear systems, profile reconstructions can be surprisingly far from the expected conductivity behavior.

Keywords: inverse problem, electromagnetic induction, Tikhonov regularization, ground conductivity, projected conjugate gradient method, *EM38*

Contents

1 Introduction

A major task of the geophysicist is to draw quantitative inferences about the Earth's interior from data collected by non-invasive and non-destructive acquisition systems.

Electromagnetic prospecting is a standard acquisition method which involves the study of fields whose space and time distribution depends on the structure and composition of the subsurface. The leading physical process here is the *skin effect* which results from the concentration of electromagnetic field near the surface of a conducting medium. At relatively high frequencies, the field at the surface depends only on electrical conductivity in the near surface, the conductivity of deeper layers being important only at lower frequencies. The electrical conductivity profile and then the Earth's crust structure can thus be determined from the measured frequency characteristics of the electromagnetic field [7].

Electromagnetic methods of geophysical prospecting, nowadays successfully used for the environmental monitoring, are strictly related to two basic investigations: the study of the general structure of the sediment sheath and the determination of local inhomogeneities of the electrical conductivity due to the presence of hidden bodies or mineral beddings.

The electromagnetic induction sensors provide estimates of the soil apparent conductivity from which the entire depth profile, among other factors a function of water content, soil salinity and clay content, must be somehow inferred. Several instruments have been developed from which a relation between recorded data and geophysical medium parameters, such as the conductivity profile, can be established through a *forward propagation model*. These instruments permit a non-invasive and a non-destructive acquisition which is, depending on the desired amount of accuracy and reliability, less expensive and faster than any other technique.

A popular method for the exploration of vadose zones and shallow aquifers is the *frequency domain electromagnetic* induction technique [12], also denoted as FEM. Applied to data acquisition at different heights above the soil, FEM technique can be used to image the electrical conductivity of the medium at different depths. Many authors claim that this method can be successfully used for the detection of a large number of different materials in the soil, also including contaminant plumes, soil water content and a large variety of industrial waste materials [10].

Different theoretical approaches have been considered to image the soil conductivity distribution from measured data.

In 1980 McNeill proposed a forward linear model, solely based on electromagnetism, for the instrumental response of the *EM38* ground conductivity meter [12], valid at low induction number (see equation (1) for its definition). Two equations are provided in which both emitting and receiving coils are either in horizontal or in vertical position. McNeill description valid for a homogeneous half space was generalized by the same author, without any experimental evidence, for stratified medium models.

Using the *EM38* ground conductivity meter and adopting the same forward model of McNeill, Borchers et al. [3] implemented a Least Squares inverse problem with second order Tikhonov regularization, to estimate electrical conductivity profiles from field data. A remarkable property of this approach is that, by opposition to other works [4, 5, 6], no further field calibration is necessary.

However, an important issue is whether McNeill's linear model is still valid in stratified field soils. Hendrickx et al. [9] claim to provide a positive answer to this question, implementing a second order Tikhonov regularization on data recorded in 14 different sites. Observing that the reconstructed conductivity profiles are mostly distant from the confidence region of the experimental data measured into the soil, is our opinion that these authors have been "lured" by the Tikhonov regularization method applied to the Least Squares minimization.

With the simple inversion problem based on McNeill's linear response model of the *EM38* ground conductivity meter, the aim of this work is to illustrate on synthetic data, how Tikhonov regularization may sometimes be the cause of misleading results, far from the expected solutions.

In conclusion to this study, the result of a conductivity profile reconstruction, derived from a data set recorded with an *EM38* ground conductivity meter, is presented and interpreted on the base of the undertaken analysis.

2 The Instrument Response Model

In this section the problem of electrical ground conductivity measurement will be presented. Some definitions will be given together with some details about the *EM38*, followed by the formulation of the linear mathematical model describing the instrument response.

2.1 McNeill's Theory

Various non-invasive and non-destructive devices can be used to acquire information from the subsurface through electromagnetic induction measurements. The instrument used in this study is the *EM38*, an electromagnetic induction sensor manufactured by Geonics Limited, Mississauga, Ontario, Canada. It consists of two coils on a lightweight bar 1 meter long, which includes calibration controls and a digital readout of apparent electrical conductivity in milliSiemens per meter (mS/m).

The *EM38* instrument operates at a frequency of $f = 14.6$ kHz which corresponds to $\omega = 91.7 \times 10^3$ rad/s. The coil spacing s is equal to 1 m. The instrument can be hold so that the two coils are either oriented horizontally or vertically with respect to the soil surface, as illustrated in Figure 1.

Alternate current is sent through the transmitter coil, this generates a magnetic field H_p which induces current to flow on the second (receiver) coil; this secondary current generates a secondary magnetic field H_s.

Defining the *skin depth* δ as the depth at which the primary magnetic field has been attenuated to $1/e$ of its original strength, we can introduce the *induction number* N_B, which is the ratio of the intercoil spacing s to the skin depth δ. For a soil with uniform conductivity σ, it can be shown that

$$N_B = \frac{s}{\delta} = s\sqrt{\frac{\mu_0\ \omega\ \sigma}{2}}. \tag{1}$$

The magnetic permeability of the free space is $\mu_0 = 4\pi \times 10^{-7}$ henry/m.

The *EM38* measures the quadrature component of the ratio of the two magnetic fields. In general this secondary magnetic field is a complicated function of the intercoil spacing s, the operating frequency f of the instruments and the ground conductivity σ. It can be shown that, under the assumption of a homogeneous medium and $N_B \ll 1$, the secondary magnetic field is a simple function of f, s and σ,

$$\frac{H_s}{H_p} \simeq \frac{\omega\ \mu_0\ \sigma\ s^2}{4}, \tag{2}$$

where $\omega = 2\pi f$ [12]. It is worthwhile mentioning that the field ratio, in the approximation provided by equation (2), is independent of the dipole orientation.

Being the ratio between the two magnetic fields linearly proportional to the electrical conductivity of the soil, the conductivity is thus evaluated by measuring this ratio. Whatever is the structure and composition of the medium under inves-

tigation, equation (2) is used to define the *apparent conductivity* σ_a, the experimental information required when solving the inverse problem of electromagnetic sounding:

$$\sigma_a = \frac{4}{\omega\,\mu_0\,s^2}\left(\frac{H_s}{H_p}\right).$$

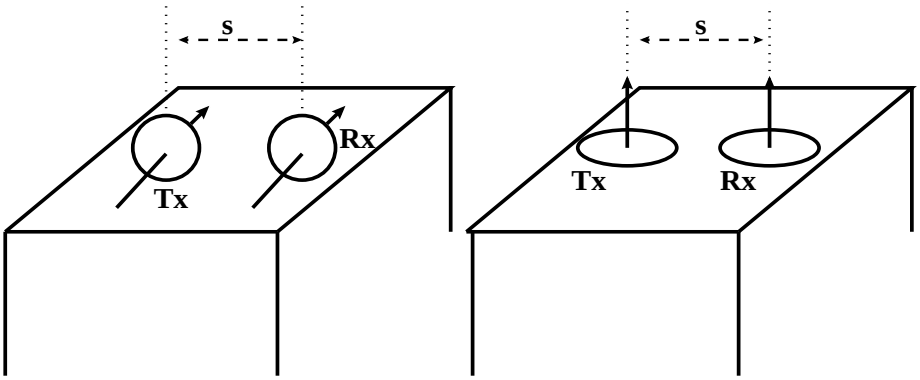

Figure 1: *Instrument configuration: horizontal (left) and vertical dipoles (right).*

Under the assumption of homogeneity and normalizing all spatial dimensions with respect to s (the intercoil spacing), McNeill in [12] is able to describe the sensitivity ϕ of the instrument to conductivity at depth z, for both vertical and horizontal modes,

$$\phi^V(z) = \frac{4z}{(4z^2+1)^{3/2}} \tag{3}$$

and

$$\phi^H(z) = 2 - \frac{4z}{(4z^2+1)^{1/2}}. \tag{4}$$

From equations (3) and (4) the apparent electrical conductivity from all material below a depth z, measured in both horizontal and vertical dipole configurations, takes the following analytical form:

$$\sigma_a(z) = \sigma \int_z^\infty \phi(y)\,dy, \tag{5}$$

where $\sigma_a(0) = \sigma$.

Figure 2 displays the sensitivity of the *EM38* for both vertical and horizontal dipole configurations, versus the depth z measured in units of distance between the

two coils. It is clear from the two sensitivity profiles, that the horizontal mode configuration is more sensitive to contributions from materials at the very near subsurface while the vertical mode configuration better discriminates contributions at lower depth, with a maximum value at about 0.4 times the distance between the coils.

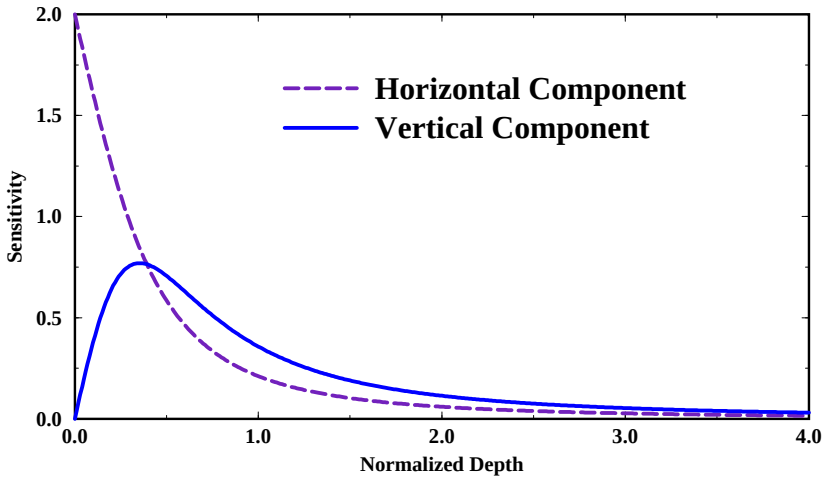

Figure 2: *Instrument sensitivity for the two dipole configurations.*

2.2 The Linear Model

From the theory developed in [12], McNeill extrapolates a more general linear model for the instrument response, based on the following assumptions:

- the subsurface model represents a horizontally stratified medium in which the current flow is entirely horizontal;
- the current flow at any point of the subsurface is independent of the current flow at any other point, since the magnetic coupling between all current loops is negligible.

Borchers et al. describe and discuss this improved model in [3]. With the two coils in vertical mode, assuming the instrument at a given *height h* above the soil,

σ_a^V takes the form

$$\sigma_a^V(h) = \int_0^\infty \phi^V(z+h)\ \sigma(z)dz, \tag{6}$$

generalizing equation (5), where $\sigma(z)$ is the conductivity at depth z. The sensitivity function $\phi^V(z)$ is described by equation (3). Similarly, for the horizontal orientation, the apparent conductivity σ_a^H is written as follows:

$$\sigma_a^H(h) = \int_0^\infty \phi^H(z+h)\ \sigma(z)dz, \tag{7}$$

with ϕ^H given by equation (4). Collecting measurements of σ_a^V and σ_a^H recorded at different elevations, $h_1, h_2, \ldots, h_N$, above the soil surface, the two integral equations (6) and (7) provide the linear forward model to invert, from which the electrical conductivity profile $\sigma(z)$ can be estimated.

Assuming a stratified medium model, see Figure 3, the subsurface is divided into M layers with specified thickness dz_j, electrical conductivity σ_j and magnetic permeability μ_j equal, in this context, to that of the free space: $\mu_j = \mu_0$, for $j = 1, 2, \ldots, M$. This last assumption is almost always true for most soils.

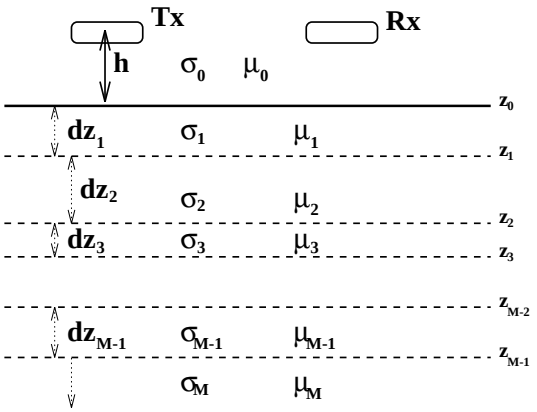

Figure 3: *Stratified subsurface model.*

Let $\mathbf{d}^T(\sigma) = [\sigma_a^V(h_1), \sigma_a^V(h_2), \ldots, \sigma_a^V(h_N), \sigma_a^H(h_1), \sigma_a^H(h_2), \ldots, \sigma_a^H(h_N)]^T$ denote the vector gathering data relative to apparent conductivity measurements,

$$\mathbf{d}(\sigma) = \begin{bmatrix} \mathbf{d^V} \\ \mathbf{d^H} \end{bmatrix}. \tag{8}$$

Using the instrument response model described by (6) and (7), the following system of linear equations establishes a correspondence between the subsurface conductivity profile and the apparent conductivity measurements:

$$\mathbf{d}(\sigma) = \mathbf{K}\sigma. \tag{9}$$

The system matrix **K** is constructed as follows,

$$\mathbf{K} = \begin{bmatrix} \mathbf{V} \\ \mathbf{H} \end{bmatrix}, \tag{10}$$

where the elements of **V** and **H** are

$$V_{i,j} = \int_{z_j}^{z_{j-1}} \phi^V(z+h_i)dz,$$

and

$$H_{i,j} = \int_{z_j}^{z_{j-1}} \phi^H(z+h_i)dz,$$

for $i = 1,2,\ldots,N$ and $j = 1,2,\ldots,M$.

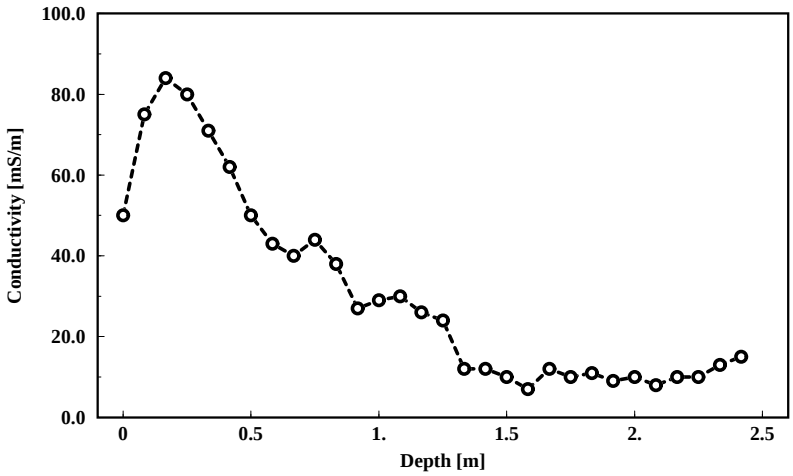

Figure 4: *Ground conductivity profile: a synthetic example.*

Figure 5 shows an example of input data vector $\mathbf{d}(\sigma)$ obtained from the electrical conductivity profile σ displayed in Figure 4, with $N = 11$ and $M = 30$. Each

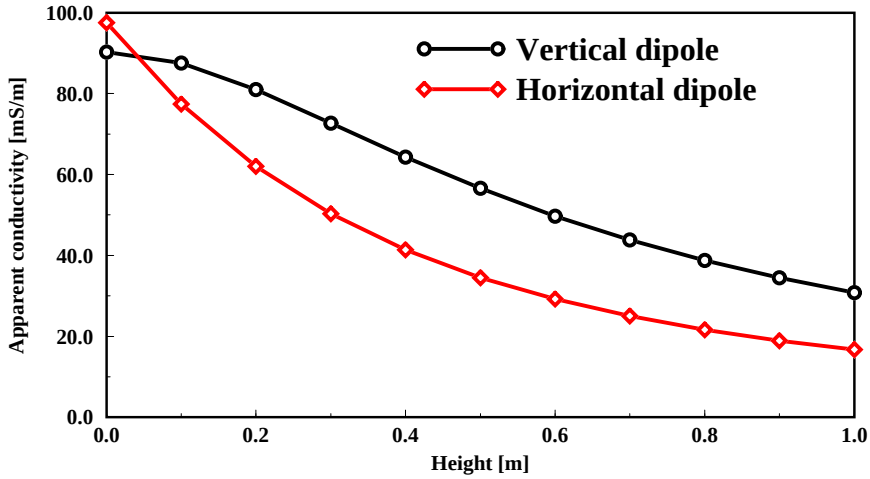

Figure 5: *Apparent conductivity: data computed from the ground conductivity profile displayed in Figure 4.*

value of the apparent conductivity was simulated for different elevations of the instrument above the soil, implementing the *forward propagation model* (9). From the $(2N \times M)$-linear system (9), the electrical conductivity profile can now be estimated from the available experimental information $\mathbf{d}$ by solving the Least Squares problem associated with the function

$$\mathcal{E}(\mathbf{s}) = \|\mathbf{K}\mathbf{s} - \mathbf{d}\|^2, \tag{11}$$

without any requirement, physical or mathematical, on the solution profile. The minimum of function $\mathcal{E}(\mathbf{s})$ is reached for an electrical conductivity profile $\mathbf{s} = \sigma$, solution of the following system:

$$\mathbf{A}\sigma = \mathbf{b}. \tag{12}$$

where $\mathbf{A} = \mathbf{K}^T\mathbf{K}$ and $\mathbf{b} = \mathbf{K}^T\mathbf{d}$. From equation (10), it follows that

$$\mathbf{A} = \mathbf{V}^T\mathbf{V} + \mathbf{H}^T\mathbf{H}\,, \tag{13}$$

where $\mathbf{A}$, an $(M \times M)$-matrix, is *symmetric* and *positive definite*. The right-hand side of (12), see equation (8), takes the form:

$$\mathbf{b} = \mathbf{V}^T\mathbf{d}^{\mathbf{V}} + \mathbf{H}^T\mathbf{d}^{\mathbf{H}}.$$

Because the instrument response σ_a depends on the *cumulative* effect of all sudden changes of the subsurface conductivity profile σ, the measured data field is weakly sensitive to the perturbations of the medium conductivity. Conversely, this physical property is mathematically translated into a strong sensibility of the inverse problem solution σ with respect to the perturbation of the apparent conductivity σ_a.

The quantity called *condition number*, defined as $\kappa(\mathbf{A}) = \lambda_M/\lambda_1$ where λ_M and λ_1 are, respectively, the largest and the smallest eigenvalue of $\mathbf{A}$, plays a prominent role as a measure of the difficulty of computing $\sigma = \mathbf{A}^{-1}\mathbf{b}$ in face of data uncertainty and roundoff errors. A classical result for non-singular operators [13] states that, for large values of $\kappa(\mathbf{A})$, the system solution σ might be *highly perturbed* even in the case of weak perturbations of both $\mathbf{A}$ and $\mathbf{b}$, or one of them. In such a situation, the problem is said to be *ill-conditioned*.

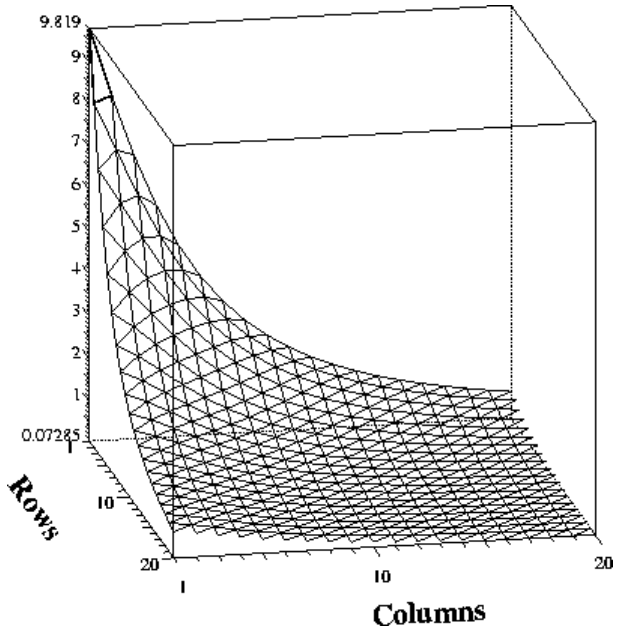

Figure 6: *Structure and coefficients of* $\mathbf{A}$*, an ill-conditioned matrix.*

Matrix $\mathbf{A}$, defined in (13) and represented in Figure 6, may be extremely ill-conditioned, depending on the depth of the subsurface one wants to investigate. In this case, where $dz_j = 0.1$ m for all $j = 1,\ldots,19$ and $dh_i = 0.1$ m for all $i = 1,\ldots,15$, the condition number $\kappa(\mathbf{A})$ is of the order of hundred of thousands.

Obviously, from the point of view of the stability, the condition number would have to be as close as possible to one.

3 The Regularization in the Sense of Tikhonov

A way to impose the stability to the inverse problem is the *Tikhonov regularization*, a method which allows a form of optimal tuning on the sensitivity of the solution to input data errors. This is obtained by the trade-off between the residual norm $\|\mathbf{K}\sigma - \mathbf{d}\|$ and some desirable property resulting from the action of a discrete differential operator $\mathbf{L}_n$ on the profile of σ. Here *n* denotes the order of the differentiation.

A perturbed solution of the inverse problem is computed by solving the Least Squares problem associated to the new function

$$\mathcal{E}_\alpha(\mathbf{s}) = \|\mathbf{K}\mathbf{s} - \mathbf{d}\|^2 + \alpha\|\mathbf{L}_n\,\mathbf{s}\|^2, \quad \alpha \geq 0. \tag{14}$$

The norm $\|\mathbf{L}_n\,\mathbf{s}\|$ quantifies the regularity of $\mathbf{s} = \sigma_\alpha$, the electrical conductivity profile that minimizes (14).

Clearly, for $\alpha = 0$, $\mathcal{E}_0$ corresponds to the function $\mathcal{E}$, equation (11), and thus the optimal conductivity is solution of the system of equations (12). In the general case, $\alpha > 0$, the minimum of $\mathcal{E}_\alpha$ is reached for the conductivity profile $\mathbf{s} = \sigma_\alpha$ solution of the linear system:

$$\widehat{\mathbf{A}}\,\sigma_\alpha = \mathbf{b}, \tag{15}$$

where $\widehat{\mathbf{A}}$, a symmetric, positive definite matrix, has the form:

$$\widehat{\mathbf{A}} = \mathbf{A} + \alpha\,\mathbf{L}_n^T\mathbf{L}_n. \tag{16}$$

$\mathbf{A}$ is defined, as before, by equation (13).

Since $\mathbf{L}_n$ is always a *diagonal dominant* matrix, the perturbing term in (16) becomes absolutely crucial to improve the conditioning of $\widehat{\mathbf{A}}$ with respect to that of $\mathbf{A}$ [1]. Hence, for $\alpha > 0$, we necessarily have $1 \leq \kappa(\widehat{\mathbf{A}}) < \kappa(\mathbf{A})$. This behavior is illustrated by the curves displayed in Figure 7.

The simplest regularizing operator is $\mathbf{L}_0 = \mathbf{I}$, where $\mathbf{I}$ denotes the identity matrix. Another form of control may be obtained through the implementation of $\mathbf{L}_2$, the second derivative operator. $\mathbf{L}_2$ enforces the smoothness of the conductivity profile while $\mathbf{L}_0$ controls its fluctuations. As illustrated in Figure 7, $\mathbf{L}_0$ provides a better conditioning to matrix $\widehat{\mathbf{A}}$.

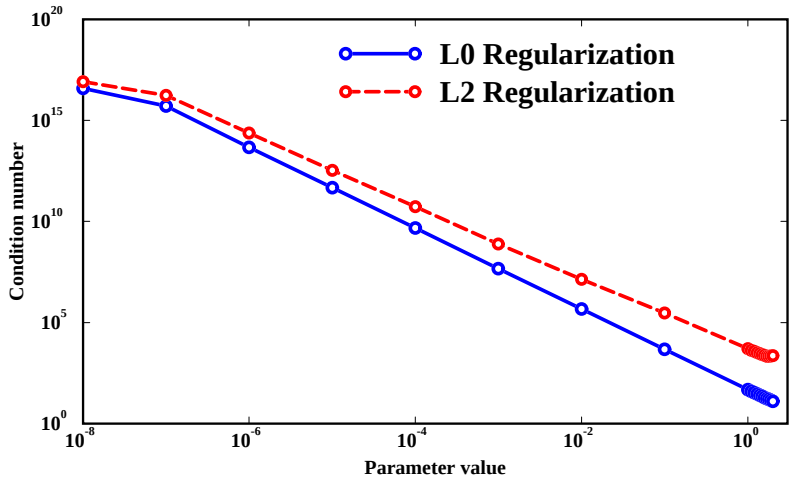

Figure 7: *Matrix regularization: condition number* $\kappa(\widehat{\mathbf{A}})$ *versus* α.

As already mentioned, the largest α, the most important the diagonal dominance of $\widehat{\mathbf{A}}$. But increasing α, the farthest the perturbed solution σ_α will be from the exact solution σ. It is then important to achieve an acceptable balance between stability and accuracy of the solution by tuning carefully the regularization parameter α.

3.1 L-curve Construction

There are several heuristic ways to operate [8, 11, 14], but the criterion described below to select α, based on the *L-curve* construction, is certainly the most used. Because the minimum of $\mathcal{E}_\alpha$ is a linear combination of two terms, $\|\mathbf{K}\sigma_\alpha - \mathbf{d}\|$ and $\|\mathbf{L}_n\sigma_\alpha\|$, the idea behind this criterion is to display one term as a function of the other for different values of the parameter α. The resulting plot is called the L-curve.

According to Tikhonov theory, for α going to zero, σ_α tends to the solution σ of the original Least Squares problem. This implies the sequence of points $(\|\mathbf{K}\sigma_\alpha - \mathbf{d}\|, \|\mathbf{L}_n\sigma_\alpha\|)$ moves along a trajectory, denoted as L-curve, presenting a limit point. This point is indicated with a cross in both examples of Figures 8 and 9, where the regularization is imposed by $\mathbf{L}_0$ and $\mathbf{L}_2$, respectively. The problem data $\mathbf{d}$ are those displayed in Figure 5. Remark that, as expected for large values

of α, the norm $\|\mathbf{L}_n\sigma_\alpha\|$ decreases while the residual $\|\mathbf{K}\sigma_\alpha - \mathbf{d}\|$ increases.

In the spirit of the L-curve criterion, the most suitable value of the regularizing parameter α is determined by selecting one intermediate point on the corner of the L-curve [8]. Such a point, indicated with a circle in Figures 8 and 9, is supposed to provide, in terms of accuracy and regularity, the value of the parameter corresponding to the most *balanced* perturbed solution of the inverse problem.

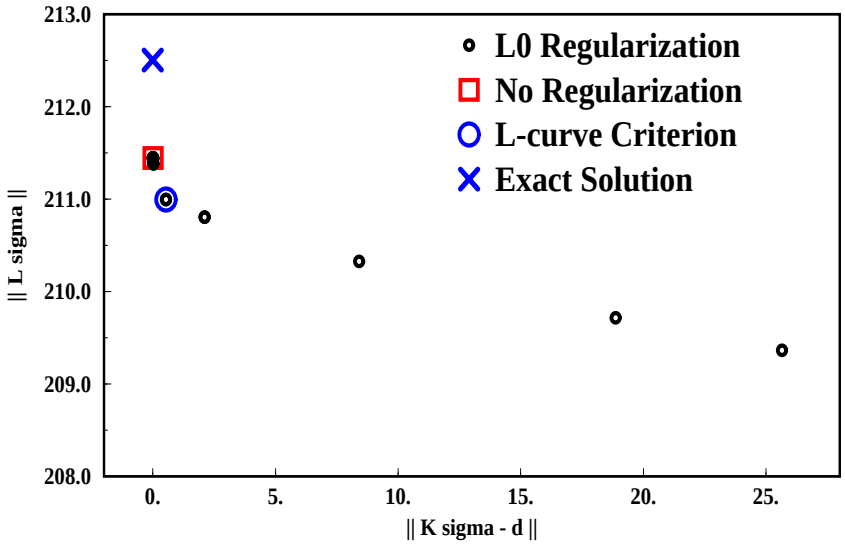

Figure 8: *Example of L-curve, 16-byte arithmetic: regularization imposed by* $\mathbf{L}_0$.

Figure 10 shows three solutions of system (15). Two of them, marked with circles in Figures 8 and 9, correspond to $\alpha = 10^{-4}$ for $\mathbf{L}_0$, and $\alpha = 4 \cdot 10^{-2}$ for $\mathbf{L}_2$. The solution profile obtained with no regularization in Figure 10 gives rise to the limit point framed by a square symbol on the L-curves.

Remark that, on the $(\|\mathbf{K}\sigma_\alpha - \mathbf{d}\|, \|\mathbf{L}_n\sigma_\alpha\|)$-plane, the point corresponding to the expected conductivity profile may be far away, above the point selected by the L-curve criterion. Although this last point represents a compromise between accuracy and regularity of the perturbed solution, the resulting α may lead to a conductivity profile σ_α which is *physically* meaningless, as illustrated in Figure 10 in the case of the $\mathbf{L}_2$ regularization.

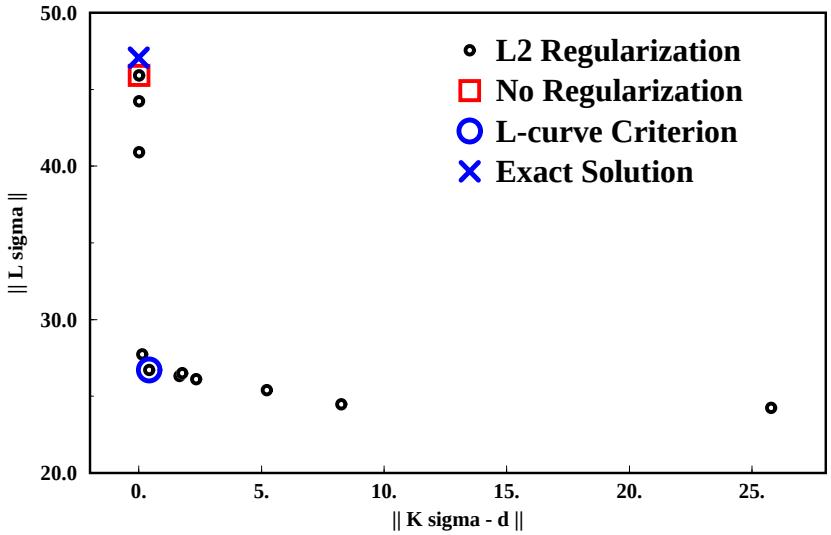

Figure 9: *Example of L-curve, 16-byte arithmetic: regularization imposed by* $\mathbf{L}_2$.

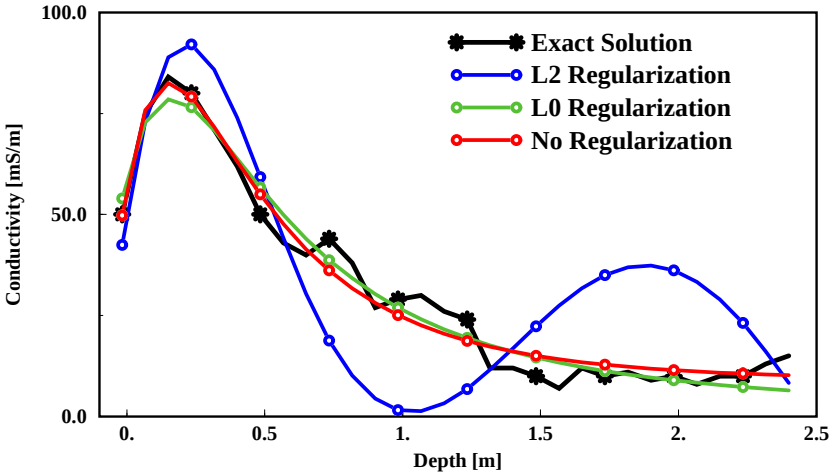

Figure 10: *Inverse problem solution for the input data shown in Figure 5.*

3.2 The Best Solution

All the computations run for the analysis illustrated in Figures 8, 9 and 10 are performed in 16-byte arithmetic, implementing a *projected* conjugate gradient algorithm [1, 2], which constrains the search of the optimal solution of the Least Square problem (14) within the feasible set $S = \{\mathbf{s} \in \mathbf{R}^M \mid \mathbf{s} \geq \mathbf{0}\}$, to satisfy the physical requirement on non-negativity of the solution (see Appendix A for a description of the algorithm implemented).

With this level of accuracy, the choice of the point on the L-curve corresponding to $\alpha = 0$ provides the best solution, in the sense of proximity to the point representing the expected solution. As a consequence, in this framework the regularization of system (12) is simply not necessary.

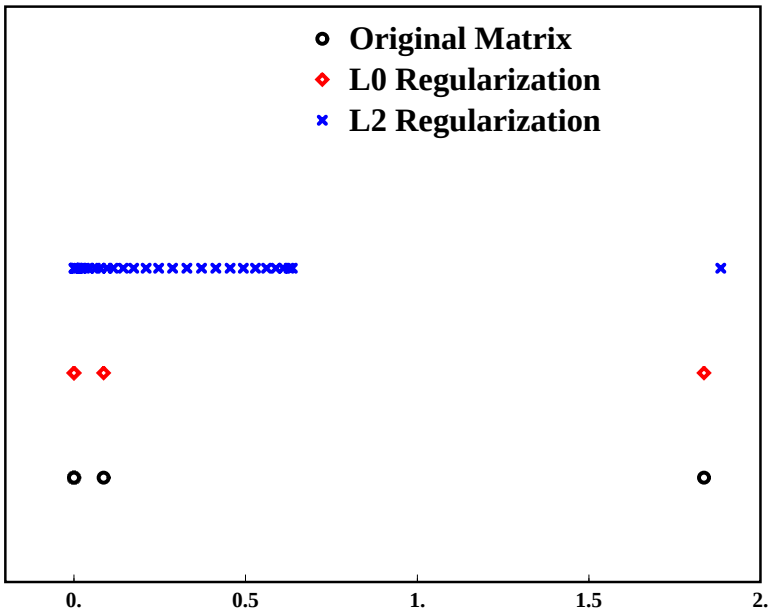

Figure 11: *Eigenvalues of* $\widehat{\mathbf{A}}$*: aggregation of values close to zero.*

As illustrated in Figure 7, problem (12) is ill-conditioned. However, the computation of the eigenvalues of $\widehat{\mathbf{A}}$, all strictly positive, shows an intriguing result concerning their aggregation close to zero, as displayed in Figure 11. In this picture, $M = 30$, the largest eigenvalue of each matrix, placed around 50, is not displayed. While the eigenvalues relative to the $\mathbf{L}_2$ regularization are spread over a large range, in the $\mathbf{L}_0$ case and in the case with no regularization, namely $\widehat{\mathbf{A}} = \mathbf{A}$,

there are only three distinct eigenvalues and the remaining group is *practically coincident* near the smallest one.

This property is of fundamental importance to obtain a fast convergence of the conjugate gradient algorithm. In particular, it can be shown that the method converges faster if most of the eigenvalues of the system matrix $\widehat{\mathbf{A}}$ are clustered in a small interval and the remaining eigenvalues lie to the right of the interval [1]. This result is eloquently illustrated by the three convergence curves presented in Figure 12. It also shows the excellent performance of the case $\alpha = 0$, in spite of the ill-conditioning of matrix $\mathbf{A}$.

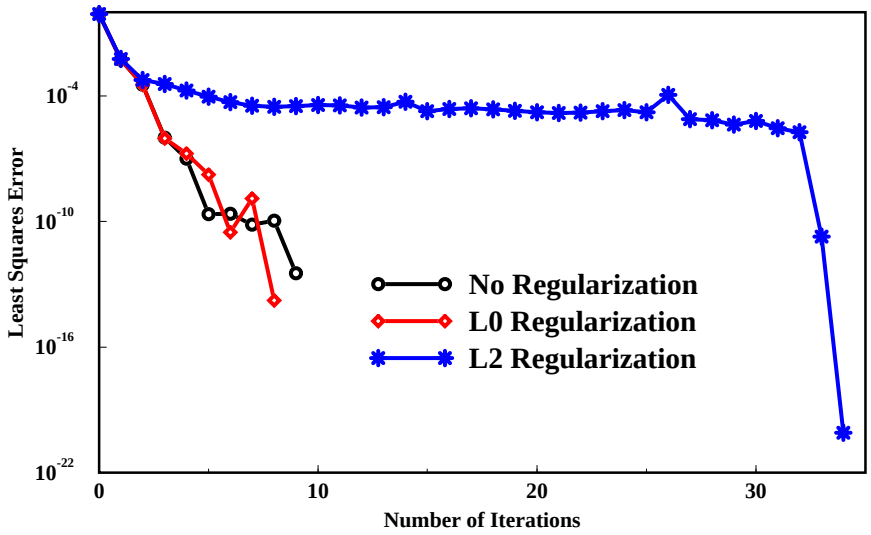

Figure 12: *Conjugate gradient: convergence history.*

Repeating a similar analysis with a 8-byte arithmetic, the same considerations about the convergence speed of the conjugate gradient hold. It is worthwhile mentioning that a careful construction of the L-curve may present values of $\alpha > 0$ providing a better solution of the Least Squares problem, in the sense of proximity to the expected solution, as shown in the example of Figure 13 where $\alpha = 10^{-12}$. Although, these values are the most suitable, the discrepancy between the resulting solutions, with respect to that corresponding to $\alpha = 0$, is practically unnoticeable.

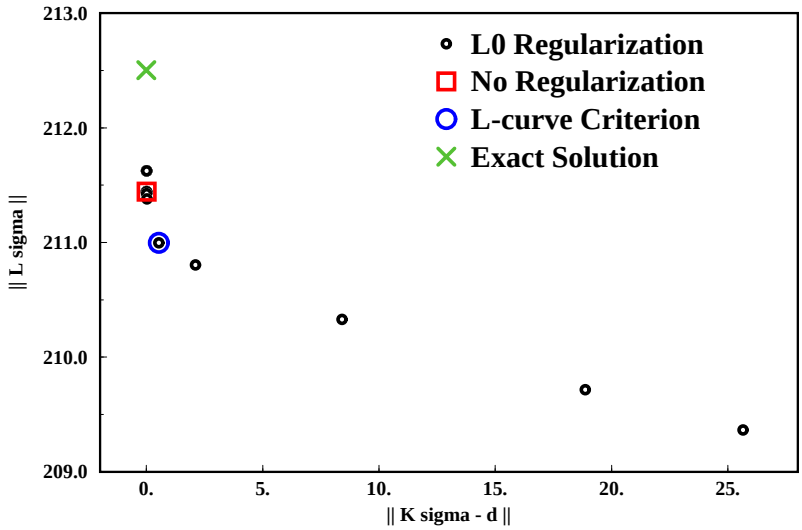

Figure 13: *Example of L-curve, 8-byte arithmetic: regularization imposed by* $\mathbf{L}_0$.

4 A Field Data Example

We tested the inversion technique, described in previous sections, on field data recorded with a Geonics *EM38* at the Poetto beach, Cagliari, Sardinia. The near-surface material of the beach, up to depths of 4-5 m, consists of unconsolidated, medium- to fine-grained sand, mainly composed by quartz (more than 60%). The sea water table, which varies during the day, is generally at a depth of about 2 m.

Five electromagnetic soundings, with a 10 m interval, were carried out along a profile orthogonal to the shore, starting 65 m from the shore itself. Each sounding was obtained by lifting the instrument above the ground and making a sequence of measurements at various heights in both vertical and horizontal coil-mode configurations. In particular, the height of the instrument varied from 0 up to 1.5 m with a 0.1 m step: for each coil position $N = 16$ readings were recorded.

Figures 14 and 15 show the resulting apparent conductivity curves as a function of height. Note that for all soundings the apparent conductivities in the vertical configuration are larger than those of the horizontal configuration. Qualitatively, this signifies the presence of a layered ground with the top layer less conductive than the underlying layers.

To quantitatively analyze these data, a subsurface layered model was defined, dividing the medium in $M = 100$ layers with $dz = 0.04$ m. Figure 16 shows the data inversion result, electrical conductivity versus depth, solution of the Least Squares problem (11). The general behavior of the conductivity curves reveals

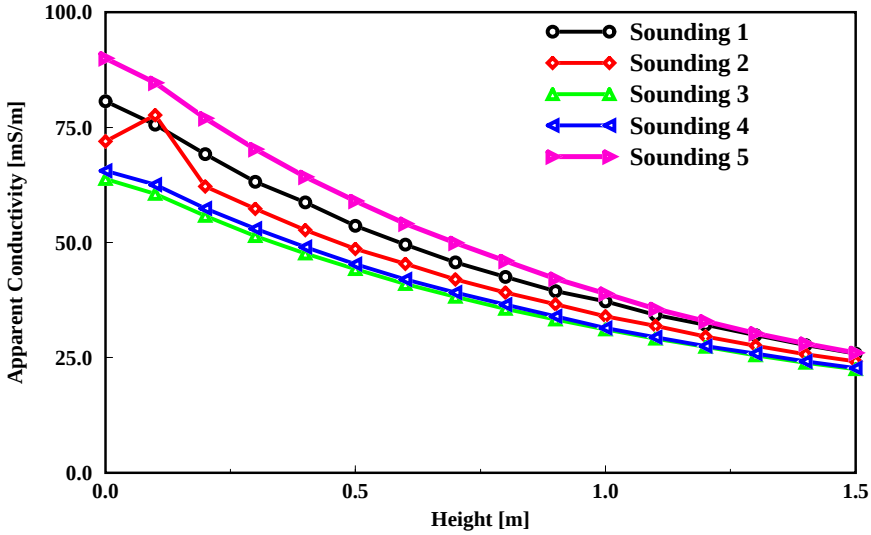

Figure 14: *Apparent conductivity,* EM38 *acquisition: vertical dipole.*

a soil profile in which three distinct zones can be evidenced. The shallowest, which extends in depth up to 0.2-0.4 m and is characterized by very low electrical conductivities, is the top layer of the beach sand. The very low conductivities of this layer are interpreted as resulting from a suspension of sand in air with porosity up to 30-40%. The deepest zone, beginning at about 1.5 m depth, is that in which the sand is fully saturated by salt water. The high conductivities prove this. Finally, the intermediate zone is the transition zone in which saturation changes from 0% to 100%.

5 Conclusions

In this article the simple inversion problem based on McNeill's linear response model of the *EM38* ground conductivity meter has been formulated and devel-

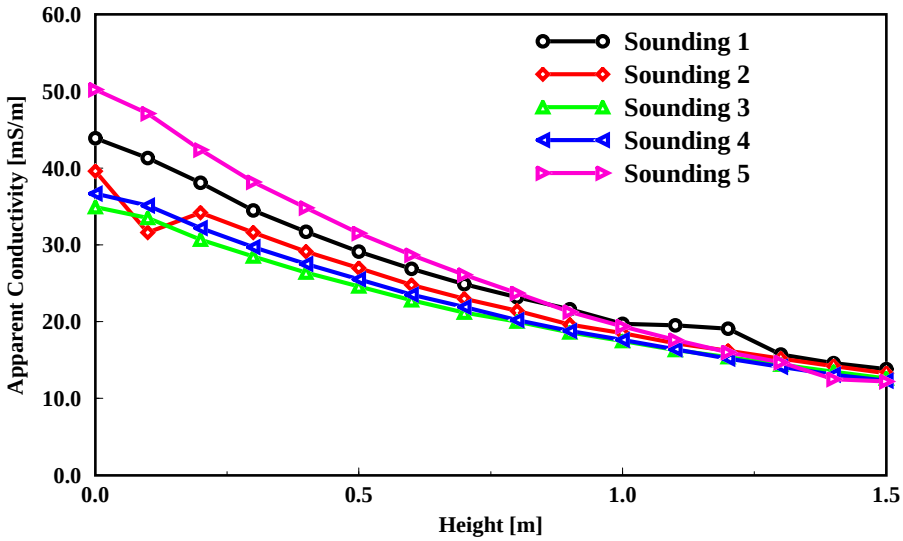

Figure 15: *Apparent conductivity,* EM38 *acquisition: horizontal dipole.*

oped. Computer experiments on both synthetic and field data provide credibility to results and conclusions presented in this work.

Computations on synthetic examples have shown how Tikhonov regularization and in particular the L-curve criterion can often be the cause of misleading conductivity profiles, far from the expected ones.

The analysis of the system matrices to invert, their structure and eigenvalues, shows that, although the original system problem (12) is ill-conditioned, the conjugate gradient algorithm is a robust method for the solution of the electrical conductivity data inversion without any additional regularization of the Least Squares problem.

The projection strategy, implemented together with the conjugate gradient, enforces the positivity of the solution and provides the best possible profile in the sense of proximity to that of the unconstrained problem.

The application to field data of the presented inversion method and the resulting interpretation prove the likelihood of the electrical conductivity reconstruction, solution of the non-regularized Least Squares problem.

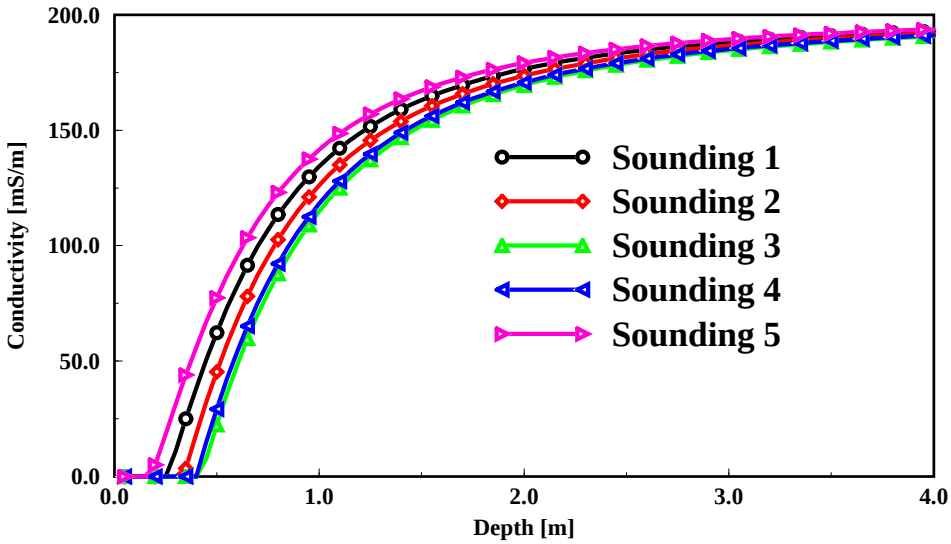

Figure 16: EM38 *acquisition: subsurface electrical conductivity profiles.*

Acknowledgment

We would like to thank Giovanni Cardone for many fruitful discussions and suggestions. The financial support of this work was provided by the Italian Ministry of the University, Project ISR8, C11-B, and by the Sardinian Regional Authorities.

Appendix

A The Projected Conjugate Gradient Algorithm

When solving the Least Squares problem (14), the solution representing the conductivity profile must satisfy the physical requirement $\sigma_\alpha \geq \mathbf{0}$. Under this condition the conjugate gradient algorithm is no longer applicable because, even if we start inside the feasible set $S = \{\mathbf{s} \in \mathbf{R}^M \mid \mathbf{s} \geq \mathbf{0}\}$, an update may take the intermediate solution outside that set. A simple remedy is to project back to the set S whenever such a situation occurs.

The conjugate gradient projection generalizes the conjugate gradient algorithm to the case where there are constraints [1, 2]. At the k-th iteration, the projection algorithm is described by the following equation:

$$\mathbf{p}_n^{(k)} = \mathcal{P}(\, \mathbf{s}_k - \lambda_n^{(k)} \mathbf{d}_n^{(k)} \,), \text{ where } \mathbf{d}_n^{(k)} = \mathbf{p}_{n-1}^{(k)} - \mathbf{s}_k \text{ and } \mathbf{d}_1^{(k)} = \mathbf{g}_k. \qquad (17)$$

$\mathcal{P}$ indicates an *orthogonal projection* operator and $\mathbf{g}_k$ the conjugate direction. In the specific case, $\mathcal{P}$ is the element-by-element projection on the constraint $s_i = 0$, for $i = 1, 2, \ldots, M$.

The parameter $\lambda_n^{(k)}$ denotes the positive step size leading the descent from the intermediate solution $\mathbf{s}_k$ to $\mathbf{y}_n^{(k)} = \mathbf{s}_k - \lambda_n^{(k)} \mathbf{d}_n^{(k)}$, the point of $\mathbf{R}^M$ minimizing the function $\mathcal{E}_\alpha$ along the line $\mathbf{d}_n^{(k)}$. The computation of $\lambda_n^{(k)}$ is usually called *line search* procedure. If the line search provides a point $\mathbf{y}_n^{(k)} \in S$, the conjugate gradient algorithm can continue the descent from the subsequent intermediate solution $\mathbf{s}_{k+1} = \mathbf{y}_n^{(k)}$.

However, as already mentioned, $\mathbf{y}_n^{(k)}$ does not necessarily lie inside the feasible set S. If this is the case, as described by equation (17), the operator $\mathcal{P}$ projects orthogonally $\mathbf{y}_n^{(k)}$ onto the boundary of S. Given $\mathbf{p}_n^{(k)}$, a new direction $\mathbf{d}_{n+1}^{(k)}$ can be individuated and, consequently, a new line search can be run. The projection procedure stops if point $\mathbf{y}_{n+1}^{(k)}$ lies in S. Figure 17 illustrates these different phases.

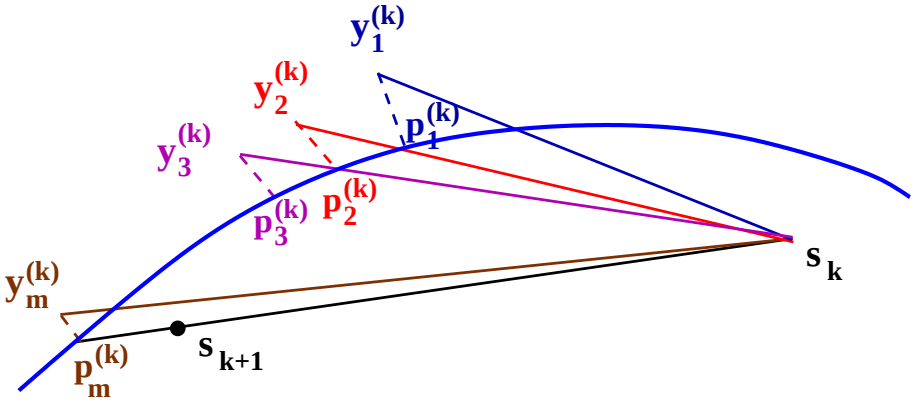

Figure 17: *A sequence of line search procedures, each one followed by a projection.*

Altogether, the convergence of the projected conjugate gradient to the solution $\mathbf{s} = \sigma_\alpha$ is guaranteed if σ_α lies in the feasible set S. Otherwise, the solution obtained represents the closest point of S with respect to σ_α.

The necessity of the projected conjugate gradient procedure reveals the inadequacy of the linear propagation model in giving a complete and coherent description of the physics. Inaccuracies in data acquisition together with errors due to computer arithmetics, can give rise to unexpected behaviors of the conjugate gradient which can take the intermediate solution outside the feasible set. The projection strategy enforces the solution to be physically acceptable and the best possible in the sense of proximity to the unconstrained one.

REFERENCES

[1] D.P. Bertsekas, J.N. Tsitsiklis, *Parallel and distributed computation: numerical methods*, Prentice Hall, 1989.

[2] E.G. Birgin, J.M. Martinez, M. Raydan, *Non-monotone spectral projected gradient methods on convex set*, SIAM Journal of Optimization, vol.10, N.4, pp.1196-1211, 1999.

[3] B. Borchers, T. Uram, J.M.H. Hendrickx, *Tikhonov regularization for determination of depth profiles of electrical conductivity using non-invasive electromagnetic induction measurements*, Soil Science Society of America Journal, N.61, pp.1004-1009, 1997.

[4] D.L. Corwin, J.D. Rhoades, *Measurements of inverted electrical conductivity profiles using electromagnetic induction*, Soil Science Society of America Journal, N.48, pp.288-291, 1984.

[5] D.L. Corwin, J.D. Rhoades, *An improved technique for determining soil electrical conductivity-depth relations from aboveground electromagnetic measurements*, Soil Science Society of America Journal, N.46., pp.517-520, 1982.

[6] P.G. Cook, G.R. Walker, *Depth profiles of electrical conductivity from linear combinations of electromagnetic induction measurements*, Soil Science Society of America Journal, N.56, pp.1015-1022, 1992.

[7] V.I. Dmitriev, E.V. Karus, *Inverse problems in geophysical prospecting*, in Ill-posed problems in the natural sciences, MIR Publishers, Moscow, A.N. Tikhonov and A.V. Goncharsky editors, 1987.

[8] P.C. Hansen, *Analysis of discrete ill-posed problems by means of the L-curve*, SIAM Review, N.34, pp.561-580, 1992.

[9] J.M.H. Hendrickx, B. Borchers, J.D. Rhoades, D.L. Corwin, S.M. Lesch, A.C. Hilgendorf, J. Schlue, *Inversion of soil conductivity profiles from electromagnetic induction measurements: theory and experimental verification*, to be published in Soil Science Society of America Journal.

[10] J.M. Hendrickx, C.D. Grande, B.A. Buchanan, R.E. Bretz, *Electromagnetic induction measurements for restoration of saline environments in New Mexico*, Waste-Management: From Risk to Remediation, chapter 13, ECM Series on Environmental Management and Intelligent Manufacturing, Vol.1, in press, R. Bhada editor.

[11] A. Hilgendorf, *Linear and nonlinear models for inversion of electrical conductivity profiles in filed coil from EM38 measurements*, MS Thesis, New Mexico Institute of Mining and Technology, 1997.

[12] J.D. McNeill, *Electromagnetic terrain conductivity measurement at low induction numbers*, Tech Note TN-6, Geonics Ltd., Ontario, Canada, 1980.

[13] V. Voievodine, *Algèbre linaire*, Traduction française, Editions Mir, Moscou, 1976.

[14] G. Wabha, *Spline models for observation data*, SIAM, Philadelphia, 1990.